Chapter 18
NMR of Paramagnetic Compounds

Yasuhiko Yamamoto and Tomokazu Shibata

Abstract Paramagnetic ions and molecules have been exploited quite extensively as extrinsic shift and relaxation probes for investigating the structure and dynamics of biological molecules. The prodigious growth of related research areas is easily discernible as the remarkably widening scope of application in diverse fields in life and material sciences. Sperm whale myoglobin (Mb) is well known as the first protein to have its three-dimensional structure revealed by X-ray crystallographic study and is also known as one of the first paramagnetic proteins studied by NMR. The heme Fe atom in Mb can exhibit a variety of oxidation, ligation, and spin states. In this chapter, Mb is selected as a reference paramagnetic compound to provide an overview of the relationship between the spectral features and the number of unpaired electrons, because the effects of a change in the spin quantum number *S*, i.e., the number of unpaired electrons, on NMR spectral parameters of a single compound can be readily understood. Field-dependent broadening of signals of proteins with a series of *S* values is also described.

Keywords Heme electronic structure · Myoglobin · Paramagnetic effect
Spin state · Unpaired electron

18.1 Introduction

The use of paramagnetic ions or molecules as extrinsic shift and relaxation probes for investigating the structures of biological molecules not only in solution, but also in solid states has been exploited much more than originally expected (see Chap. 15) [1–45]. In addition, dynamic nuclear polarization (DNP) ascribing to the magnetization transfer occurring from unpaired electrons to nuclei through stochastic

Y. Yamamoto (✉) · T. Shibata
Department of Chemistry, University of Tsukuba, Tsukuba 305-8571, Japan
e-mail: yamamoto@chem.tsukuba.ac.jp

T. Shibata
e-mail: shibata@chem.tsukuba.ac.jp

The Nuclear Magnetic Resonance Society of Japan, *Experimental Approaches of NMR Spectroscopy*, https://doi.org/10.1007/978-981-10-5966-7_18

modulation of the hyperfine interaction between electron and nuclear spins (see Chap. 4) is gaining increasing attention for a variety of applications, showing its potential in solution and solid-state NMR as well as in MRI [38, 46–49]. NMR study of paramagnetic compounds originated in solid-state physics in the middle of the 1950s [50, 51], and as is well known, the technique was soon introduced to chemistry and biochemistry. By 1970, the physical principles underlying the technique were well understood and the basic concepts of the technique, together with the theoretical framework for interpreting NMR parameters of paramagnetic compounds, had been well established [1, 2, 10, 52–61]. The prodigious growth of related research areas is easily witnessed by the remarkably widening scope of application in diverse fields in life and material sciences. A large number of reviews on NMR study of paramagnetic compounds have already appeared, some [10, 19, 62–64] comprehensive and others [3–9, 11–18, 20, 21, 23, 26–29, 38, 40, 65] more focused. Considering the aim of the present book, this chapter should serve as a reference source for active researchers and as an introduction to this subject for a novice, with particular emphasis on the experimental aspects. In view of the multiple purposes of the chapter, we selected hemoproteins, particularly sperm whale myoglobin [Mb (Fig. 18.1a)], as reference compounds. As is well known, Mb was the first protein to have had its three-dimensional structure revealed by X-ray crystallographic study [66]. Mb is also known as one of the first paramagnetic proteins studied by NMR [67], and paramagnetic hemoproteins such as Mb, cytochrome *c*, and hemoglobin were extensively investigated by Shulman [68], Wüthrich [69], Ogawa [70], La Mar [71], and Morishima [72] during the late 1960s to the late 1970s. In addition, paramagnetic Mb has been used for one of the landmark NMR measurements, which demonstrated that, in a magnetic field-oriented molecule, a

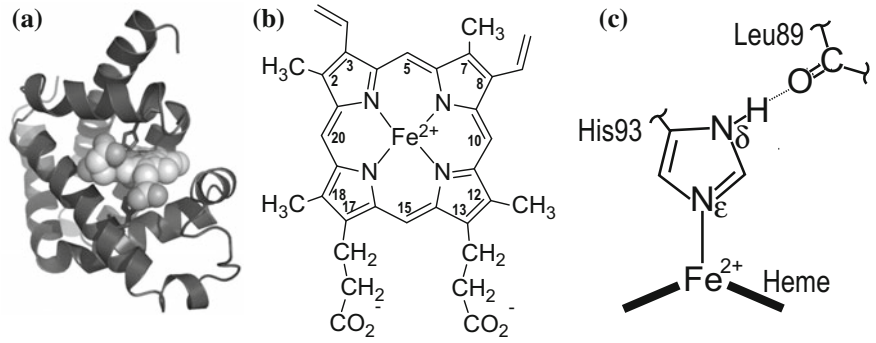

Fig. 18.1 **a** Schematic representation of the structure of sperm whale myoglobin (Mb; Protein Data Bank ID 1A6M). The polypeptide chain is illustrated as a ribbon model, and the heme is drawn as a space-filling model. **b** Structure and numbering system of heme. **c** Schematic drawing of the heme coordination structure in deoxy Mb [76]. The hydrogen bonding interaction of His93 $N_\delta H$ with the Leu89 carbonyl oxygen atom is represented by a broken line

magnetic dipole–dipole interaction does not average to zero [73] and yields a measurable dipolar coupling useful for refinement of structural and dynamic properties of molecules [74].

Mb is an oxygen (O_2) storage hemoprotein with a molecular weight of about 17 kDa [75]. The heme cofactor (Fig. 18.1b) is buried inside the protein matrix composed of 153 amino acid residues, and its binding to the protein is stabilized by the coordination bond between the heme iron (Fe) atom and the nitrogen one (N_ε) of the proximal His (His93) [66, 76–78] (Fig. 18.1c), together with hydrophobic interaction of the heme cofactor with the surrounding amino acid residues in the heme pocket and the formation of salt bridges between the heme propionate groups and nearby polar amino acid side chains [76–78]. The heme Fe atom in Mb is generally in either the ferrous (Fe^{2+}) or ferric (Fe^{3+}) state. The numbers of electrons in the 3*d* orbitals of Fe^{2+} and Fe^{3+} are six and five, respectively (inset of Fig. 18.2). Hence, the total spin quantum number *S* is the integer and half-integer for Fe^{2+} and Fe^{3+}, respectively. Depending upon the degree of spin pairing of electrons in the 3*d* orbitals, Fe^{2+} can have 4, 2, or 0 unpaired electrons, corresponding to $S = 2$, 1, or 0, respectively, and Fe^{3+} corresponding to 5, 3, or 1 unpaired electron, $S = 5/2$, 3/2, or 1/2, respectively. Based on an octahedral ligand field, the energy levels of the five 3*d* orbitals are split into two groups in such a way that the levels of the d_{z^2} and $d_{x^2-y^2}$ orbitals are higher than those of the other three orbitals, d_{xy}, d_{yz}, and d_{xz}. The spin state of Mb depends on the chemical nature of the ligand. For heme Fe^{2+}, the deoxy form (deoxy Mb) is penta-coordinated with a high-spin configuration, $S = 2$, and the oxy form (MbO_2) or carbonmonoxy form (MbCO) possesses a low-spin configuration, $S = 0$. On the other hand, the binding of ligands of relatively weak field strength such as H_2O to heme Fe^{3+} gives high-spin state $S = 5/2$ [metMb(H_2O)], and low-spin state $S = 1/2$ is obtained with a strong ligand such as CN^- [metMb(CN^-)]. In addition, the binding of ligands of intermediate field strength such as N_3^- [metMb(N_3^-)] exhibit a thermal equilibrium between $S = 1/2$ and $S = 5/2$ states. Complexes with $S = 1$ and 3/2 are not so common and have been obtained in some particular systems such as Fe^{4+}-peroxo species ($S = 1$) and Fe^{3+} species coupled with O_2^- ($S = 3/2$) [79].

Aside from the importance of Mb in the early history of the NMR study of paramagnetic compounds, the significance of Mb in NMR studies is mainly twofold, as follows. Firstly, as described above, the heme Fe atom in Mb can exhibit a variety of oxidation, ligation, and spin states, and hence, the effects of a change in the *S* value, i.e., the number of unpaired electrons, on NMR spectral parameters of a single compound, can be readily understood. Secondly, the relationship between the contact shift (δ_c), due to a delocalized unpaired electron, and a pseudo-contact one (δ_{pc}), due to a through-space dipolar interaction with the unpaired electron spin(s), as to paramagnetic shift (δ_{para}) is clearly reflected in the spectra of paramagnetic Mbs, and thus, a comprehensive description of the δ_c value can be given in terms of delocalization of unpaired electron density from the paramagnetic center. We intend to portray a range of techniques applied to paramagnetic Mbs, which exhibit widespread utility in life and material sciences.

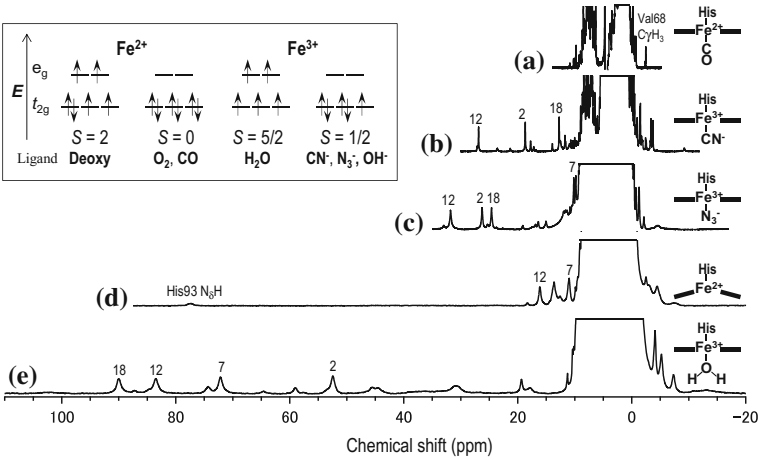

Fig. 18.2 400 MHz ^{1}H NMR spectra of **a** carbonmonoxy form [Mb(CO)], **b** met-cyano form [metMb(CN^{-})], **c** met-azido form [metMb(N_3^{-})], **d** deoxy form (deoxy Mb) of Mb in 90% $^{1}H_2O$/10% $^{2}H_2O$, pH 7.4, at 25 °C, and **e** met-aquo form [metMb(H_2O)] of the protein in 90% $^{1}H_2O$/10% $^{2}H_2O$, pH 6.5, at 25 °C. The heme Fe oxidation and ligation states of the proteins are schematically illustrated on the right-hand side of the spectra. The assignments of heme methyl proton signals, i.e., 2-, 7-, 12-, and 18-CH_3, are indicated by the corresponding numbers in the spectra. In (**a**), four signals are observed at ~3 ppm. In (**b**), the 7-CH_3 signal at ~5 ppm is buried in the diamagnetic envelope, and in (**d**), 2- and 18-CH_3 signals are not assigned yet. Assignments of the Val68 $C_\gamma H_3$ signal of Mb(CO) and the His93 $N_\delta H$ proton signal of deoxy Mb are also indicated. In *the inset*, typical heme Fe oxidation, spin, and ligation states of the protein are illustrated. The intermediate spin complexes, i.e., Fe^{2+} S = 1 and Fe^{3+} S = 3/2 complexes, are obtained in some particular systems [79]

18.2 Paramagnetic Effects

The theory behind NMR parameters in paramagnetic systems has been treated thoroughly elsewhere [2, 10, 13, 16]. Only a qualitative description of paramagnetic shifts and relaxation, which will suffice to allow an appreciation of the spectra presented, is given below.

18.2.1 Paramagnetic Shifts

Analysis of δ_{para} in terms of the interaction between nuclear and electron spins provides a wealth of information about electronic and molecular structures [2, 8–21]. The observed shift (δ_{obs}) of a paramagnetic compound is given as in Eq. (18.1), where δ_{dia} and δ_{para} are the diamagnetic and paramagnetic contributions, respectively.

$$\delta_{obs} = \delta_{dia} + \delta_{para} \tag{18.1}$$

δ_{dia} is the shift that would have been observed if the molecule contained no unpaired electron, and δ_{para} is expressed as the sum of δ_c and δ_{pc},

$$\delta_{para} = \delta_c + \delta_{pc} \tag{18.2}$$

δ_c reflects the electronic structure of the molecule, and the metal-centered δ_{pc}, due to the magnetic dipolar field arising from delocalized unpaired electron(s) at the paramagnetic center, has been used extensively to refine the molecular structure (see Chap. 15 of this book).

In addition to δ_{para} itself, its temperature dependence also provides valuable information about the molecule. Since both δ_c and δ_{pc} are proportional to the reciprocal of absolute temperature (T), plots of δ_{obs} against $1/T$, often called Curie plots, exhibit a straight line with the intercept at $1/T \rightarrow 0$, which is equal to δ_{dia}. However, anomalous Curie plots are occasionally observed, and the thermodynamic nature of the thermal spin equilibrium in metMb(N_3^-) [80] and the thermal equilibrium between ^5E, $(d_{xy})(d_{xz})^2(d_{yz})(d_{z^2})(d_{x^2-y^2})$, and $^5B_2$, $(d_{xy})^2(d_{xz})(d_{yz})(d_{z^2})(d_{x^2-y^2})$, states of high-spin heme Fe^{2+} in deoxy Mb [81], have been quantitatively characterized through analysis of such anomalous temperature-dependent shift changes of the signals.

18.2.2 Paramagnetic Relaxation

The analysis of nuclear relaxation has provided a wealth of information about the structural and dynamic properties of molecules. In particular, in the case of paramagnetic metalloproteins, the dynamic nature of a molecule is sharply manifested in paramagnetic relaxation observed for paramagnetically shifted NMR signals [2, 10, 13, 14, 16].

The nuclear relaxation rate (R_{obs}) in a paramagnetic system is expressed as the sum of diamagnetic (R_{dia}) and paramagnetic (R_{para}) terms,

$$R_{obs} = R_{dia} + R_{para} \tag{18.3}$$

R_{dia} is the sum of the contributions of the dipole–dipole interaction (R_{dia}^{DD}), chemical shift anisotropy (R_{dia}^{CSA}), and others (R_{dia}^{other}),

$$R_{dia} = R_{dia}^{DD} + R_{dia}^{CSA} + R_{dia}^{other}. \tag{18.4}$$

The contributions of R_{dia}^{CSA} to the nuclear spin–lattice (R_{1dia}) and spin–spin (R_{2dia}) relaxation rates (R_{1dia}^{CSA} and R_{2dia}^{CSA}, respectively) depend on the magnetic field strength and can be written as follows [56],

$$R_{1\mathrm{dia}}^{\mathrm{CSA}} = \frac{6}{40}\omega_I^2\delta_z^2\left(1+\frac{\eta^2}{3}\right)J(\omega_I) \tag{18.5}$$

$$R_{2\mathrm{dia}}^{\mathrm{CSA}} = \frac{1}{40}\omega_I^2\delta_z^2(3J(\omega_I)+4J(0)) \tag{18.6}$$

$$J(\omega_I) = \frac{2\tau_r}{1+\omega_I^2\tau_r^2}, \tag{18.7}$$

where δ_z is associated with the principal components of the chemical shift tensor, η is the asymmetric parameter of the molecule under consideration, and $J(\omega_I)$ represents the spectral density function.

On the other hand, R_{para} is expressed as the sum of the contributions of metal-centered ($R_{\mathrm{para}}^{\mathrm{MC}}$) and ligand-centered ($R_{\mathrm{para}}^{\mathrm{LC}}$) dipolar terms, the contact hyperfine interaction ($R_{\mathrm{para}}^{\mathrm{C}}$), and Curie spin relaxation ($R_{\mathrm{para}}^{\mathrm{Curie}}$) [2], as illustrated in Fig. 18.3,

$$R_{\mathrm{para}} = R_{\mathrm{para}}^{\mathrm{MC}} + R_{\mathrm{para}}^{\mathrm{LC}} + R_{\mathrm{para}}^{\mathrm{C}} + R_{\mathrm{para}}^{\mathrm{Curie}}. \tag{18.8}$$

Using the Solomon–Bloembergen equations [52, 82], together with the expression of $R_{\mathrm{para}}^{\mathrm{Curie}}$ [83, 84] (see Chap. 15 of this book), paramagnetic

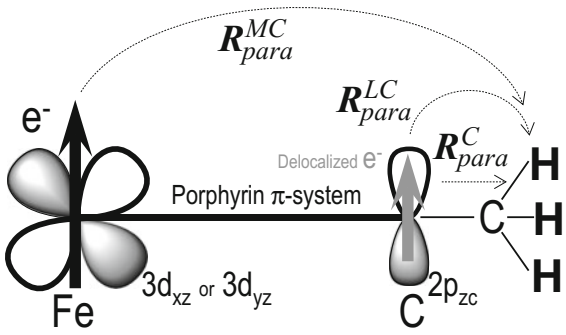

Fig. 18.3 Schematic representation of paramagnetic relaxation mechanisms for heme CH_3 protons. Paramagnetic metal-centered relaxation ($R_{\mathrm{para}}^{\mathrm{MC}}$) is due to the dipole–dipole interaction between the nuclear spin and electron spin localized at heme Fe. Paramagnetic ligand-centered relaxation ($R_{\mathrm{para}}^{\mathrm{LC}}$) is due to the dipole–dipole interaction between the nuclear spin and electron spins delocalized from heme Fe into the ligand atoms, and, in the case of the heme CH_3 proton, $R_{\mathrm{para}}^{\mathrm{LC}}$ due to the electron spin delocalized into the p_z orbital of the carbon atom to which CH_3 is covalently attached is predominant. Paramagnetic contact relaxation ($R_{\mathrm{para}}^{\mathrm{C}}$) arises from the contact hyperfine interaction between the nuclear spin and electron spin delocalized into the 1 *s* orbital of the CH_3 hydrogen atoms. Curie spin relaxation ($R_{\mathrm{para}}^{\mathrm{Curie}}$) arises from the dipole–dipole interaction between the nuclear spin and the time average of the electron magnetic moment (not shown)

contributions to the nuclear spin–lattice and spin–spin relaxation rates ($R_{1\text{para}}$ and $R_{2\text{para}}$, respectively) in a paramagnetic system are expressed by

$$\begin{aligned} R_{1\text{para}} = {} & \frac{2}{15}\left(\frac{\mu_0}{4\pi}\right)^2 \gamma_I^2 \beta_e^2 \mu_B^2 S(S+1)\left(\gamma_M^{-6} + \Sigma\rho^2\gamma_L^{-6}\right) \\ & \times \left[\frac{\tau_{c2}}{1+(\omega_I-\omega_S)^2\tau_{c2}^2} + \frac{3\tau_{c1}}{1+\omega_I^2\tau_{c1}^2} + \frac{6\tau_{c2}}{1+(\omega_I+\omega_S)^2\tau_{c2}^2}\right] \\ & + \frac{2}{3}S(S+1)\left(\frac{A}{\hbar}\right)^2\left[\frac{\tau_{e2}}{1+(\omega_I+\omega_S)^2\tau_{e2}^2}\right] \\ & + \frac{2}{5}\left(\frac{\mu_0}{4\pi}\right)^2 \frac{\omega_I^2\beta_e^4\mu_B^4 S^2(S+1)^2}{(3kT)^2 r_M^6}\left(\frac{3\tau_r}{1+\omega_I^2\tau_r^2}\right) \end{aligned} \tag{18.9}$$

$$\begin{aligned} R_{2\text{para}} = {} & \frac{1}{15}\left(\frac{\mu_0}{4\pi}\right)^2 \gamma_I^2 \beta_e^2 \mu_B^2 S(S+1)\left(\gamma_M^{-6} + \Sigma\rho^2\gamma_L^{-6}\right) \\ & \times \left[4\tau_{c1} + \frac{3\tau_{c2}}{1+(\omega_I-\omega_S)^2\tau_{c2}^2} + \frac{3\tau_{c1}}{1+\omega_I^2\tau_{c1}^2} + \frac{6\tau_{c2}}{1+\omega_S^2\tau_{c2}^2} + \frac{6\tau_{c2}}{1+(\omega_I+\omega_S)^2\tau_{c2}^2}\right] \\ & + \frac{1}{3}S(S+1)\left(\frac{A}{\hbar}\right)^2\left[\tau_{e1} + \frac{\tau_{e2}}{1+(\omega_I-\omega_S)^2\tau_{e2}^2}\right] \\ & + \frac{1}{5}\left(\frac{\mu_0}{4\pi}\right)^2 \frac{\omega_I^2\beta_e^4\mu_B^4 S^2(S+1)^2}{(3kT)^2 r_M^6}\left(4\tau_{c2} + \frac{3\tau_r}{1+\omega_I^2\tau_r^2}\right) \end{aligned} \tag{18.10}$$

$$\tau_{c1}^{-1} = T_{1e}^{-1} + \tau_r^{-1} + \tau_{\text{ex}}^{-1} \tag{18.11}$$

$$\tau_{c2}^{-1} = T_{2e}^{-1} + \tau_r^{-1} + \tau_{\text{ex}}^{-1} \tag{18.12}$$

$$\tau_{c1}^{-1} = T_{1e}^{-1} + \tau_{\text{ex}}^{-1} \tag{18.13}$$

$$\tau_{c2}^{-1} = T_{2e}^{-1} + \tau_{ex}^{-1}, \tag{18.14}$$

where, in the present case, r_M and r_L are the distances between the proton of interest and the Fe atom, and between the proton and the pyrrole carbon atom, respectively, ρ is the unpaired electron density at the pyrrole carbon atoms (Fig. 18.1b), $\left(\frac{A}{\hbar}\right)$ is the apparent hyperfine coupling constant, ω_I and ω_S are the Larmor frequencies of the nucleus and electron, respectively, T_{1e} and T_{2e} are the electron longitudinal and transverse relaxation times, respectively, and τ_{ex} is the electron exchange time. The other parameters are as usual. In large molecules with highly resolved NMR spectra, $T_{1e}, T_{2e} \ll \tau_r$, and at high magnetic field, $\omega_I^2 T_{1e}^2 \ll 1$, $1 < \omega_S^2 T_{1e}^2$, and $1 < \omega_S^2 T_{2e}^2$, Eqs. (18.7) and (18.8) are reduced to the following equations [85, 86]

$$R_{1\text{para}} = \frac{2}{15}\left(\frac{\mu_0}{4\pi}\right)^2 \gamma_I^2 \beta_e^2 \mu_B^2 S(S+1)\left(\gamma_M^{-6} + \Sigma\rho^2\gamma_L^{-6}\right) T_{1e} \tag{18.15}$$

$$\begin{aligned} R_{2\text{para}} = {} & \frac{7}{15}\left(\frac{\mu_0}{4\pi}\right)^2 \gamma_I^2 \beta_e^2 \mu_B^2 S(S+1)\left(\gamma_M^{-6} + \Sigma\rho^2\gamma_L^{-6}\right) T_{1e} \\ & + \frac{1}{3}S(S+1)\left(\frac{A}{\hbar}\right)^2 T_{1e} + \frac{4}{5}\left(\frac{\mu_0}{4\pi}\right)^2 \frac{\omega_I^2 \beta_e^4 \mu_B^4 S^2 (S+1)^2}{(3kT)^2 r_M^6}\tau_r \end{aligned} \tag{18.16}$$

Equation (18.16) dictates that $R_{2\text{para}}$ depends on the field strength due to the contribution of $R_{\text{para}}^{\text{Curie}}$, the third term on the right-hand side of the equation (see Sect. 18.4.2).

18.3 ^{1}H NMR Spectra of Myoglobin with 0, 1, 4, or 5 Unpaired Electrons

In this section, ^{1}H NMR spectra of Mbs in a variety of oxidation, ligation, and spin states are overviewed to understand the relationship between the number of unpaired electrons and the spectral features. In addition, 400, 600, and 800 MHz ^{1}H spectra of each form of the protein are compared with each other to observe the field dependence of the spectral parameters.

18.3.1 Overview

400 MHz ^{1}H spectra of Mb(CO), metMb(CN^-), metMb(N_3^-), deoxy Mb, and metMb(H_2O) are shown in Fig. 18.2. Heme methyl (CH_3) proton signals are often used as sensitive probes for the heme electronic structures of hemoproteins [6, 14]. In addition to ready observation of the signals with three-proton intensity, the δ_{para} values of the hemoprotein provide a measure of the nonequivalence of the four pyrrole environment of the porphyrin ring, i.e., the in-plane asymmetry of the heme electronic structure, because there is a CH_3 group on each pyrrole (Fig. 18.1b), and delocalization of unpaired electron(s) from the heme π-system to the s orbital of the CH_3 protons necessary for the Fermi contact interaction occurs effectively through hyperconjugation [2, 10]. Comparison of the δ_{para} values of the heme CH_3 proton signals between heme model compounds and hemoproteins in every oxidation/spin state indicated that the spread of the four signals is always much larger in the protein environment [6]. The spread of the four heme CH_3 proton signals in model compound is due to intrinsic in-plane asymmetry of the heme electronic structure, and hence, the increase in the spread of the signals in the protein reflects the asymmetric nature of the heme–protein linkage, which is relevant to regulation of heme Fe reactivity, and hence the protein function [2, 6, 14].

In the presence of a large spread of the four heme CH_3 proton signals, the average shift of the signals is used as a measure of the electronic nature of the heme Fe atom in the protein. The average shift of the signals of diamagnetic Mb(CO) is ~3 ppm [87] (trace 2a), and those of paramagnetic metMb(CN^-) and metMb(H_2O) are ~14 [88] and ~75 ppm [89, 90], respectively (traces 2B and E, respectively). Thus, the average shift of the paramagnetically shifted heme CH_3 proton signals is roughly proportional to the number of unpaired electrons, i.e., the S value. The average shift of the signals of metMb(N_3^-), i.e., ~23 ppm [91] (trace 2c), is somehow between those of metMb(CN^-) and metMb(H_2O), because of the intermediate ligand field strength of N_3^-, which renders the energy difference between the Fe^{3+} low-spin (S = 1/2) and high-spin (S = 5/2) states comparable to the thermal energy [91–94]. Finally, among the physiologically active forms of the protein, deoxy Mb is the least understood in terms of the molecular properties of its heme active site [81, 95–97]. Despite extensive efforts, the ground-state electronic structure of the Fe^{2+} high-spin (S = 2) state of deoxy Mb remains to be elucidated [81]. Due to out-of-plane displacement of the Fe atom from the porphyrin plane in the penta-coordinated heme complex in the protein [77] (Fig. 18.1c), the average shift of the four heme CH_3 proton signals of deoxy Mb, i.e., ~15 ppm [96], is rather small, while the signal of the axial His93 $N_\delta H$ proton is observed at ~77 ppm [98] (trace 2d).

18.3.2 Diamagnetic Carbonmonoxy Form [Mb(CO)]

Mb(CO) is often considered as a model of Mb(O_2) that tends to be spontaneously oxidized to metMb(H_2O) through a reaction known as autoxidation. In the absence of a unpaired electron, Mb(CO) is just like an ordinary diamagnetic protein. So the benefit of the higher resolution in the spectrum recorded at higher magnetic field strength can be clearly witnessed in Fig. 18.4. The ring current effect of the porphyrin moiety of heme is considerably greater than that of the phenyl group of such as phenylalanine. As a result, the Val68 $C_\gamma H_3$ proton signal is resolved at ~ −2.5 ppm [99], and signals due to heme 5, 10, 15, and 20-H protons (Fig. 18.1b) are resolved in a downfield-shifted region, i.e., >~9.5 ppm [87]. Hence, the porphyrin π-system of heme itself can be considered as a sort of intrinsic shift reagent. Furthermore, some NH protons involved in intramolecular hydrogen bonding are also resolved below ~9.5 ppm [99, 100].

18.3.3 Paramagnetic Deoxy Form (Deoxy Mb) with S = 2

The His93 $N_\delta H$ proton signal is resolved at ~77 ppm [98] and the heme CH_3 proton ones in the range of <~20 ppm [96] (trace 2d). The line widths of signals due to the His93 $N_\delta H$ and heme CH_3 protons of the protein in a 400 MHz spectrum

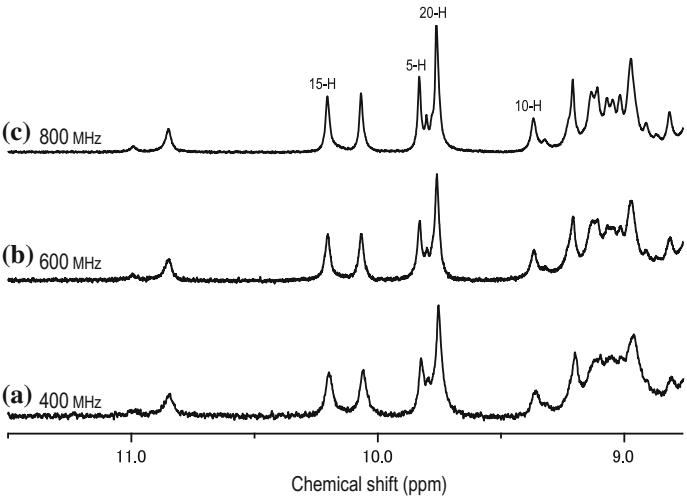

Fig. 18.4 Portions, 8.8–11.5 ppm, of ^{1}H NMR spectra of Mb(CO) in 90% $^{1}H_2O$/10% $^{2}H_2O$, pH 7.4, at 25 °C, recorded at ^{1}H frequencies of 400 (**a**), 600 (**b**), and 800 MHz (**c**). Assignments of *meso* 5-, 10, 15-, and 20-H proton (see Fig. 18.1b) signals are indicated in (**c**). The signals resolved below ∼9.5 ppm are due to NH protons involved in intramolecular hydrogen bonding [99, 100]

at 25 °C (trace 2d) are ∼450 and ∼120 Hz, respectively, and their relaxation times are <∼10 ms. Consequently, as far as acquisition of only the paramagnetically shifted signals of the protein is concerned, the repetition time can be set considerably short, provided that the experimental setting is properly optimized. A drawback to such a measurement is that it will distort the spectral features of signals due to protein protons far away from the paramagnetic center because of the long relaxation times. A relatively large number of dummy scans prior to data acquisition will help to reduce the spectral distortion caused by short repetition times.

The unpaired electrons of the heme Fe atom of deoxy Mb are delocalized into the His93 imidazole through the Fe–His σ and π bonds, i.e., σ- and π-delocalization, respectively [2, 10, 101]. The delocalization of the positive spin of an unpaired electron through the σ- and π-delocalization results in a net spin density of the opposite sign, that is, negative, and a positive spin on the His93 N_{ε} atom, respectively, and the spin on the His93 N_{ε} atom is further delocalized, through the π system of the imidazole ring, into the N_{δ} atom, and then finally into the 1*s* orbital of the His93 $N_{\delta}H$ hydrogen, through σ spin polarization [102]. As a result, the positive spin is delocalized into the 1*s* orbital of the His93 $N_{\delta}H$ hydrogen through σ-delocalization, whereas the negative spin is delocalized through π-delocalization. Thus, the δ_c value for the His93 $N_{\delta}H$ shift is determined as the difference between the σ- and π-delocalization, and hence, large positive δ_c values

indicate that the σ-delocalization dominates over the π-delocalization [101]. The strength of the Fe–His bond is possibly affected by steric and electronic factors. La Mar and de Ropp [103] demonstrated, in a study involving horse radish ferrous peroxidase, that the proximal His $N_\delta H$ proton shift is greatly affected by the hydrogen bond between the $N_\delta H$ proton and a protein acceptor residue through its effect on the delocalization of the unpaired electron along the N_δ–H bond, and that simultaneous consideration of changes of the stretching frequency of the Fe–His bond [104] and the axial His $N_\delta H$ proton shift enables differentiation of the steric and electronic influences on the Fe–His bond [103]. In the case of deoxy Mb, the delocalization of the unpaired electron from the N_δ atom to the 1*s* orbital of the $N_\delta H$ hydrogen decreases with increasing strength of the His93–Leu89 H-bond because the interaction between the $N_\delta H$ hydrogen and the unpaired electron density on the His93 imidazole ring is hampered by enhancement of polarization of the charge in the N_δ–H bond. Furthermore, a change in the strength of the His93–Leu89 hydrogen bond (Fig. 18.1c) also influences the Fe–His bond strength in such a manner that the Fe–His bond becomes stronger with increasing His93–Leu89 hydrogen bond strength because of enhancement of the Fe ← His σ donation. Consequently, the strengthening of the Fe–His bond through an increase in the His93–Leu89 H-bond strength results in an increase in the stretching frequency of the Fe–His bond and, inversely, a decrease in the His93 $N_\delta H$ shift [103].

In contrast to effective delocalization of unpaired electrons from the heme Fe atom to the His93 imidazole π system through the Fe–His bond, unpaired electron density delocalized from the Fe atom into the porphyrin π system in the penta-coordinated heme complex is considerably smaller than that in a hexa-coordinated one such as metMb(H_2O) (see Sect. 18.3.6) due to the relatively weak electronic interaction between the Fe orbitals and the porphyrin π system in the former complex [102]. As a result, the heme CH_3 proton signals of deoxy Mb exhibit relatively small δ_{para} values. In addition, the Val68 $C_\gamma H_3$ proton signal is resolved in upfield-shifted region, i.e., $< \sim -7$ ppm [100], in the ^1H spectrum of deoxy Mb, due to magnetic anisotropy of the Fe^{2+} high-spin state [95].

The signals of deoxy Mb increased dramatically with increasing the field strength (Fig. 18.5), and the field-dependent broadening was enhanced for signals of larger paramagnetic molecules [105]. According to the theory proposed by Gueron [83], there will be net polarization of the Fe electron spin magnetic moment that will be oriented along the direction of the external magnetic field. Modulation of this dipolar field due to the spin polarization (known as the "Curie spin") through rotational diffusion will then introduce an extra field-dependent term into the expression for transverse relaxation (Eq. 18.16). Since the Curie spin contribution is proportional to the square of the magnetic field strength [83, 84], the benefit of higher resolution in a spectrum recorded at higher magnetic field strength is no longer expected for deoxy Mb.

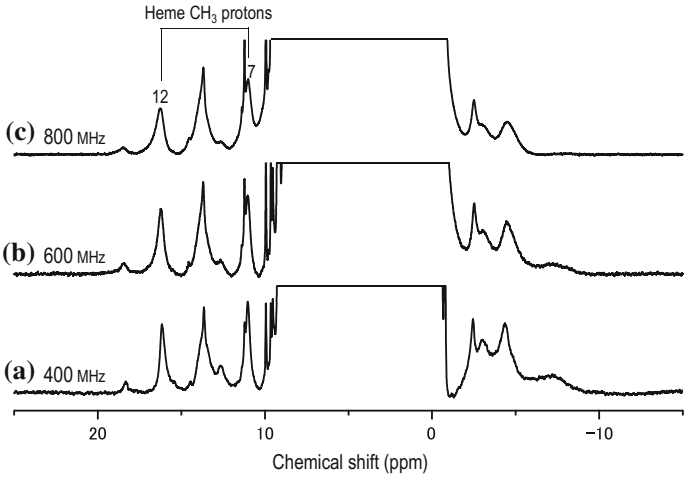

Fig. 18.5 Portions, −15 to 25 ppm, of ^{1}H NMR spectra of deoxy Mb in 90% $^{1}H_2O$/10% $^{2}H_2O$, pH 7.4, at 25 °C, recorded at ^{1}H frequencies of 400 (**a**), 600 (**b**), and 800 MHz (**c**). Assignments of heme 7- and 12-CH_3 signals are indicated in (**c**) [96]

18.3.4 Paramagnetic Met-Cyano Form [MetMb(CN⁻)] with S = ½

Owing to the short spin–lattice relaxation time of electron (T_{1e}), i.e., $\sim 2 \times 10^{-12}$ s [4, 20], and the large magnetic anisotropy of hexa-coordinated Fe^{3+} heme complexes with $S = 1/2$ [106], metMb(CN^-) exhibits well-resolved and relatively narrow signals useful for characterizing the electronic/molecular structure of its heme active site [14, 106]. The asymmetric nature of the heme–protein linkage can be readily characterized through analysis of the δ_{para} values of the four heme CH_3 proton signals of metMb(CN^-). The energy levels for the d_{xz} and d_{yz} orbitals are affected by the interaction with axial ligands, and a single unpaired electron resides in either the d_{xz} or d_{yz} orbital, whichever possesses the highest energy. Consequently, depending upon the relative energy of the d_{xz} and d_{yz} orbitals, π spin delocalization occurs into either pyrroles I, III or II, IV (Fig. 18.6). Since a diatomic cyanide ion is coordinated to the heme Fe atom with its orientation nearly normal as to the heme plane, its coordination does not affect the degree and pattern of the in-plane asymmetry of the heme electronic structure. Consequently, the energy levels for the d_{xz} and d_{yz} orbitals are predominantly affected by the orientation of the His93 imidazole ring, relative to the heme, through a repulsive interaction between the p_z orbital of the Fe-bound nitrogen atom of His93 imidazole and the d_{xz} or d_{yz} one of the heme Fe atoms (Fig. 18.6a). The Fe–His coordination bond is roughly along the heme normal, and hence, with the orientation of His93 imidazole, as shown in Fig. 18.6a [107], i.e., the projection of the His93 imidazole ring onto the heme plane is along the nitrogen atoms of pyrroles I and II, and the p_z orbital of the

Fe-bound nitrogen atom in the yz plane interact repulsively with the d_{yz} one, raising the energy level of d_{yz} orbital relative to that of the d_{xz} one (Fig. 18.6b). Consequently, the unpaired electron spin density delocalized from heme Fe atom into the pyrroles I and III π-system is much greater than that into pyrroles II and IV one, due to the unpaired electron delocalized from the singly occupied d_{yz} orbital directly to the former pyrroles. In contrast, the energy level of the d_{xz} orbital is higher than that of the d_{yz} one with the orientation of the His93 imidazole ring, of which the projection onto the heme plane is along the nitrogen atoms of pyrroles I and III, and the unpaired electron spin density delocalized from the heme Fe atom into the pyrroles II and IV π-system is greater than that into the pyrroles I and III one (Fig. 18.6c). Since the orientation of the His93 imidazole ring in Mb is similar to that illustrated in Fig. 18.6a [76, 77], the δ_c values of the signals due to the heme CH_3 groups at positions 2 and 12 are larger than those at positions 7 and 18.

The large magnetic anisotropy of metMb(CN^-) induces large δ_{pc} values for signals arising from protons located close to the heme Fe atom, as can be witnessed by the observation of many resolved signals due to amino acid protons (Fig. 18.7). The combined use of NMR and X-ray studies allows determination of principal components and orientation, with respect to the heme, of the magnetic susceptibility tensor in the protein [106]. Formulation of the δ_{pc} value is useful for detailed characterization of the local structure. In addition, due to the small Curie spin relaxation expected from the small S value, the signals of metMb(CN^-) exhibit

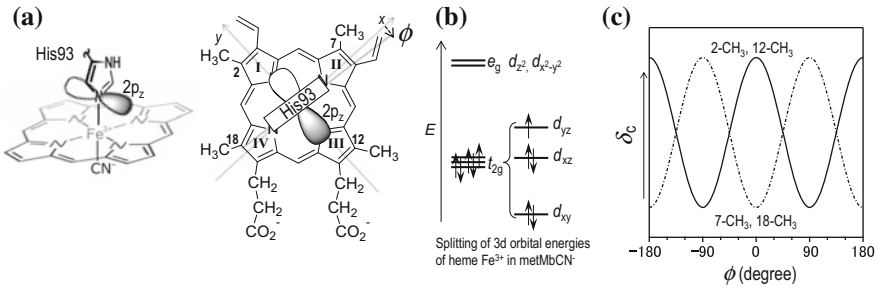

Fig. 18.6 **a** Schematic representation of the orientation of the His93 imidazole ring and $2p_z$ orbital of the His93 N_ε atom, with respect to the heme in Mb [76, 77]. Heme peripheral side chains are eliminated for clarity. Angle ϕ is defined as the angle between the projection of the His93 imidazole plane onto the heme one and the N_{II}–Fe–N_{IV} axis. **b** Splitting of 3*d* orbital energies of heme Fe^{3+} in metMbCN$^-$. With $\phi = \sim 0°$, the energy level of the $3d_{yz}$ orbital is higher than that of the $3d_{xz}$ one. Hence, electron spin density delocalized from the heme Fe atom into the pyrroles I and III π-system is much greater than that into the pyrroles II and IV one, due to unpaired electron delocalized from the singly occupied d_{yz} orbital directly to the former pyrroles. Coordination of CN^- with its orientation nearly normal to the heme plane does not significantly affect the energy levels of the $3d_{yz}$ and $3d_{xz}$ orbitals. **c** Semi-quantitative representation of ϕ dependence of the contact shift (δ_c) of heme 2- and 12-CH_3 (*solid line*), and 7- and 18-CH_3 (*alternate long* and *short dash line*) signals of metMbCN$^-$. The δ_c value was estimated with the assumption of fourfold symmetry in the electronic structure of the porphyrin moiety of heme

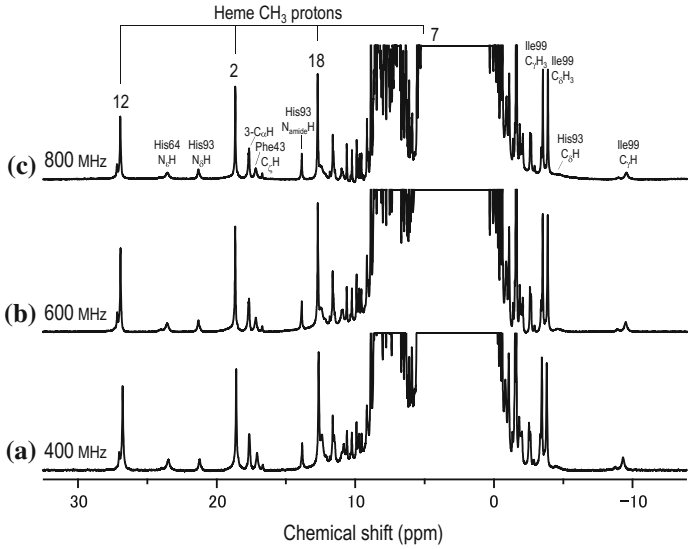

Fig. 18.7 Portions, −13.9 to 32.5 ppm, of ^{1}H NMR spectra of metMb(CN^{-}) in 90% $^{1}H_2O$/10% $^{2}H_2O$, pH 7.4, at 25 °C, recorded at ^{1}H frequencies of 400 (**a**), 600 (**b**), and 800 MHz (**c**). Assignments of heme CH_3 and some amino acid proton signals are indicated in (**c**)

small field-dependent broadening, i.e., the line widths of heme 12-CH_3 signals recorded at 400, 600, and 800 MHz were 39, 44, and 66 Hz, respectively (Fig. 18.7).

18.3.5 Paramagnetic Met-Azido Form [MetMb(N_3^-)] with Mainly S = ½

The met-azido derivatives of hemoproteins in general share the property that they exhibit a thermal equilibrium between low-spin, S = 1/2, and high-spin, S = 5/2, states, due to the intermediate field strength of N_3^- [92, 93]. Hence, changes in the population of the two spin states in the equilibrium provide a sensitive probe of the effective axial field strength. Among various techniques used to characterize the thermal spin equilibria in proteins, NMR is probably the most sensitive one and provides two separate probes of the average spin magnetization of the heme Fe atom, i.e., the heme CH_3 proton and axial His93 $N_\delta H$ proton δ_{para} values [80, 91]. The thermal spin equilibrium in metMb(N_3^-) is manifested in the curvature or anti-Curie behavior of Curie plots, i.e., the plots of the δ_{obs} values against the reciprocal of absolute temperature (1/T), of these signals [80, 91]. Fitting of the Curie plots using the van't Hoff equation provides thermodynamic parameters of the equilibrium [80]. In the case of metMb(N_3^-), the high-spin contents at ambient

temperature are ∼20%, and the values of ∼−13 kJ mol^{-1} and ∼−30 J T^{-1} mol^{-1} have been reported for the enthalpy change (ΔH) and molar entropy (ΔS), respectively [105]. ΔH is simply determined by the difference in thermodynamic energy between the low-spin and high-spin states, and ΔS is determined by the structural and dynamic natures of the heme environment. The appreciable contribution of the high-spin state to the ground-state electron configuration of heme Fe^{3+} in metMb(N_3^-) leads to sizable Curie spin relaxation, which considerably broadens paramagnetically shifted signals with increasing magnetic field strength, e.g., the line width of the heme 12-CH_3 signal at 25 °C was ∼140 Hz at 400 MHz, ∼160 Hz at 600 MHz, and ∼200 Hz at 800 MHz (Fig. 18.8).

18.3.6 *Paramagnetic Met-Aquo Form [MetMb(H_2O)] with* S = 5/2

In the presence of five unpaired electrons in the system, the signals of metMb(H_2O) are observed over the range of ∼110 to ∼−30 ppm [89, 90]. Although the signals are considerably broad due to its relatively long T_{1e}, i.e., $<\sim 1 \times 10^{-10}$ s [4, 20], owing to the large chemical shift range, the signals are fairly well separated (Fig. 18.9). In Fe^{3+} high-spin complexes, the relaxation process for the heme proton signals is modulated mainly by T_{1e}, which is in turn determined by modulation of the zero-field level of the complex [108, 109]. Some Mbs possess penta-coordinated

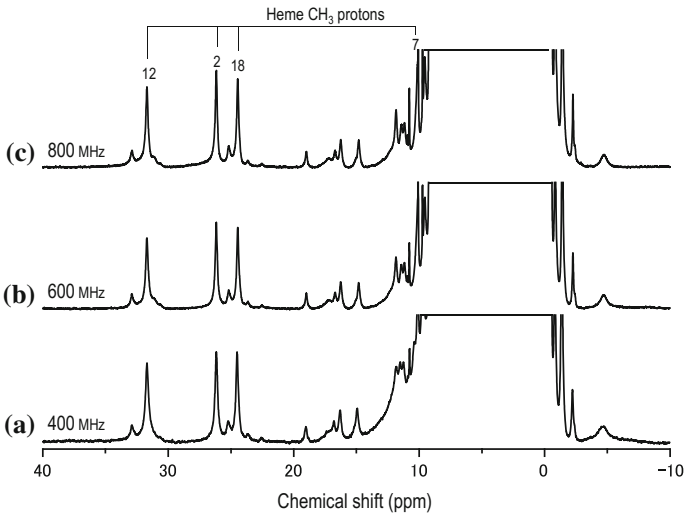

Fig. 18.8 Portions, −10 to 40 ppm, of ^1H NMR spectra of metMb(N_3^-) in 90% ^1H_2O/10% ^2H_2O, pH 7.4, at 25 °C, recorded at ^1H frequencies of 400 (**a**), 600 (**b**), and 800 MHz (**c**). Assignments of heme CH_3 signals are indicated in (**c**)

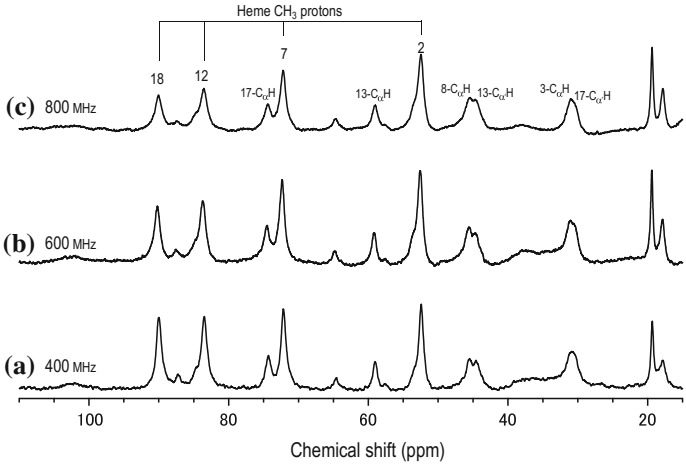

Fig. 18.9 Portions, 15–110 ppm, of ^{1}H NMR spectra of metMb(H_2O) in 90% $^{1}H_2O$/10% $^{2}H_2O$, pH 7.0, at 25 °C, recorded at ^{1}H frequencies of 400 (**a**), 600 (**b**), and 800 MHz (**c**). Assignments of heme side chain proton signals are indicated in (**c**)

hemes in their Fe^{3+} high-spin complexes because of the absence of Fe-bound H_2O [110]. The heme proton signals of the Mbs with penta-coordinated Fe^{3+} high-spin hemes are narrower than those of the proteins with hexa-coordinated ones, because of the larger zero-field splitting in the former hemes, due to the lower symmetry in the ligand field around the heme Fe, which leads to the reduction of T_{1e} [110].

As indicated in trace 2e, signals resolved outside of the so-called diamagnetic envelope, i.e., ∼10 to ∼0 ppm, are mostly due to heme peripheral side chain protons, and only a few signals due to amino acid protons are resolved. These spectral features indicated that δ_c is large, while δ_{pc} is relatively small. The δ_{pc} contribution of metMb(H_2O) is due to magnetic anisotropy caused by zero-field splitting at the heme Fe and is in practice axially symmetric [111]. Since the Curie spin relaxation contribution is significant in high-spin metMb(H_2O), the line widths of paramagnetically shifted signals increased dramatically with increasing magnetic field strength, e.g., the line width of the heme 12-CH_3 signal at 25 °C was ∼380 Hz at 400 MHz, ∼560 Hz at 600 MHz, and ∼950 Hz at 800 MHz (Fig. 18.9).

18.4 NMR Measurements

18.4.1 NOEs in Paramagnetic Compounds

Despite the initial prejudice that the presence of unpaired electron(s) in paramagnetic molecules seriously diminishes the magnitude of NOEs through

"paramagnetic leakage," and hence the observation of NOEs in paramagnetic systems is practically unrealistic, nowadays NOE measurements have been extensively applied for signal assignments and structural characterization in various paramagnetic systems [17]. The observation of relatively large NOEs in paramagnetic systems [88, 90, 107, 112, 113] could be rationalized on the basis of the nature of relaxation in the systems. The steady-state NOE in an isolated two-spin is given by Eq. (18.17)

$$\mathrm{NOE}_{i\to j} = \frac{\sigma_{ij}}{\rho_j} \tag{18.17}$$

where σ_{ij} and ρ_j are the cross relaxation rate between the interacting protons, i and j, and the intrinsic spin–lattice relaxation rate of spin j, respectively. For paramagnetic system, $\rho_j = \rho_{\mathrm{dia}} + \rho_{\mathrm{para}}$ (ρ_{dia} and ρ_{para} are the diamagnetic and paramagnetic contributions to ρ_j, respectively), and for a dominant paramagnetic relaxation ($\rho_{\mathrm{dia}} \ll \rho_{\mathrm{para}}$), the steady-state NOEs are considerably reduced through paramagnetic leakage. Although the magnitude is relatively small, the observation of NOEs has been reported for most accessible oxidation and spin states of proteins.

Since σ_{ij} is given by

$$\sigma_{ij} = \frac{\hbar^2\gamma_H^2}{10r^6}\left[\frac{6\tau_\mathrm{c}}{1+4\omega_H^2\tau_\mathrm{c}^2} - \tau_\mathrm{c}\right] \tag{18.18}$$

where γ_H is the gyromagnetic ratio of proton, r is the distance between the protons, τ_c is the correlation time that modulates the dipolar interaction between the two spins, and ω_H is the Larmor frequency of proton. In the case of macromolecules, at high magnetic field and a long τ_c, the molecular motion occurs in the slow motion limit ($\omega_H^2\tau_c^2 \gg 1$), and Eq. (18.19) is reduced to

$$\sigma_{ij} = -\frac{\hbar^2\gamma_H^2\tau_\mathrm{c}}{10r^6} \tag{18.19}$$

Thus, the magnitude of the NOEs is simply proportional to τ_c, and hence, as far as σ_{ij} is concerned, the observation of NOEs could be more promising for a larger molecule than for a small one. In practice, however, for a diamagnetic system with a large τ_c, the detrimental effects of spin diffusion preclude the collection of any useful data in NOE studies. However, as demonstrated by La Mar and coworkers [90], paramagnetism not only undermines spin diffusion, and hence allows observation of specific NOEs for larger systems, but also improves the magnitude of NOEs with increasing τ_c. Consequently, a large molecular size is likely to be an advantage rather than a disadvantage for observing useful NOEs in a paramagnetic system (Fig. 18.10).

The optimization of experimental parameters in 1D and 2D NOE measurements on rapidly relaxing systems, where σ_{ij} is much smaller than ρ_j, has been fully

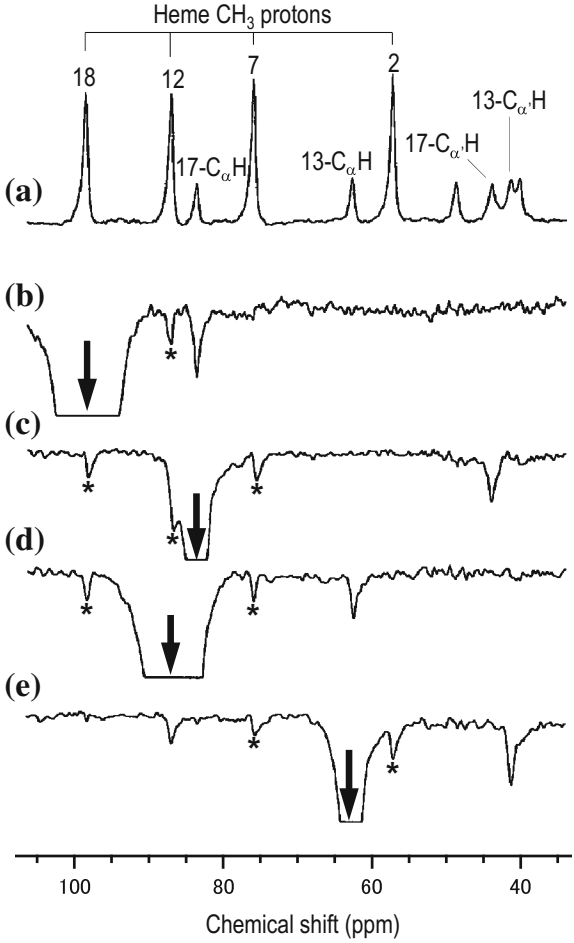

Fig. 18.10 Downfield-shifted portions, 33–108 ppm, of the 500 MHz ^{1}H NMR spectrum and NOE difference spectra of shark *Galeorhinus japonicas* metMb in $^{2}H_2O$, pH 7.0, at 35 °C. **a** Reference spectrum and (**b**–**e**) NOE difference spectra generated by subtracting the reference spectrum (**a**) from the spectrum recorded with saturation of the desired signal. *Arrows* indicate signals that are saturated, and peaks due to the decoupler pulse power spillage are indicated by *asterisk*. **b** Saturation of the 18-CH_3 signal exhibiting an NOE to a 17-C_αH one. **c** Saturation of 17-C_αH signal exhibiting an NOE to 17-$C_{\alpha'}$H one. **d** Saturation of the 12-CH_3 signal exhibiting an NOE to a 13-C_αH one. **e** Saturation of the 13-C_αH signal exhibiting an NOE to a 13-$C_{\alpha'}$H one. The spectra were taken from [91]

discussed [17, 90]. Considering $\sigma_{ij} \ll \rho_j$ in a paramagnetic system, the magnitude of NOEs to be detected is quite small. In the spectrum of a paramagnetic molecule, fast relaxing signals exhibit large δ_{para} and hence are resolved outside of the diamagnetic envelope. The observation of NOEs between a rapidly relaxing signal and a slowly relaxing one, resonating in the diamagnetic envelope, can be much more

effectively performed by conventional 1D NOE difference spectroscopy, provided that the signal-to-noise ratio of spectra is high enough to detect small NOEs. The accumulation of a large number of transients is a simple and easy approach to achieve a satisfactory signal-to-noise ratio. A short acquisition time due to a large spectral width and a relatively low digital resolution generally used for the observation of the spectra of a paramagnetic system, together with rapid repetition owing to fast paramagnetic relaxation, significantly contributes to effective data collection. In general, the detection of a small intensity change becomes more difficult as the signal broadens. Hence, T_2 is often the determining factor for observing the effect; since $T_2 \leq T_1$, this is particularly true for signals with short T_1s.

Practically, there are also other limitations to the NOE method applied to paramagnetic systems. First, when saturating a fast relaxing signal by decoupler irradiation, the necessarily strong decoupler RF field irradiation can induce interfering off-resonance perturbations over a wide region of the spectrum [90]. In such a case, true NOEs may be difficult to distinguish from an off-resonance effect, often called "decoupler power spillage." Comparison of the relative magnitudes of the effects under conditions of a reduced off-resonance effect and the determination of the actual power profile, as a function of offset, of the decoupler RF field irradiation can usually alleviate the problem. Second, observation of a small intensity difference in a broad signal demands a high dynamic range for the receiver and the digitizer. Selective excitation pulse sequences such as a simple 1–1 jump and return one [114] are helpful for suppressing the diamagnetic signals and allowing the full utilization of the dynamic range.

18.4.2 Hydrogen Exchange Rates

Biological macromolecules exhibit freedom of various structural changes, which are often relevant to their functions. Consequently, in order to elucidate the functions of the molecules, their static structures described by X-ray crystallographic coordinates must be augmented by their dynamic properties manifested in various spectroscopic data. Among a variety of spectroscopic techniques available for studies of their dynamic nature, NMR is quite unique in terms of not only its sensitivity as to dynamic structures exhibiting a wide range of timescales, but also its ability to provide information from which detailed descriptions of the dynamic structures of molecules in solution can be made.

Upon such dynamic studies involving NMR, it is important to consider the "NMR timescale." For example, in the case of a molecule with interconvertible conformations, i.e., conformers I and II, which possibly exhibit two distinct NMR signals, whether or not we can observe two separate signals due to conformers I and II depends on the timescale of the interconversion. If the interconversion is sufficiently slow compared with the NMR timescale, signals I and II can be separately observed. On the other hand, if the interconversion is faster than the NMR timescale, a single signal representing the time-averaged conformation of conformers I

and II is observed. The NMR timescale of the interconversion between conformers I and II is given by the difference in resonance frequency between signals I and II ($\Delta\delta_{I/II}$) and hence depends on magnetic field strength (B_0) in such a manner that the NMR timescale increases with increasing B_0 because $\Delta\delta_{I/II}$ is proportional to B_0. Taking advantage of the large δ_{para}, a paramagnetic counterpart possibly exhibits the $\Delta\delta_{I/II}$ value that is large enough to allow observation of separate signals I and II. Thus, the NMR timescale can be controlled through the paramagnetic effect.

The exchange rates (k_{ex}) of labile protons provide a wealth of information about the structural and functional features of proteins. For example, the X-ray structures of Mb [76, 77] suggested that the equilibrium structure does not possess channels large enough to permit ligand entry to and exit from the heme cavity. Theoretical calculations [115] have shown that the protein backbone and side chain motions of Mb modulate the energy barrier for O_2 entry. Thus, the dynamics, as well as the structure of a protein, are relevant to its function [116, 117]. One of the most powerful methods for studying protein dynamics is the observation of the exchange behavior of labile protons, which are buried in the protein interior [118–120]. The timescale of exchange of labile protons can be considered as a measure of the local dynamic stability [116–120].

k_{ex} is derived from solvent saturation transfer from the intrinsic spin–lattice relaxation time [$T_{1(int)}$] and the saturation factor (F) given by [121]

$$F = \frac{I}{I_0} = T_{1(int)}^{-1} \times \left(T_{1(int)}^{-1} + \tau_i^{-1}\right)^{-1} \tag{18.20}$$

where I and I_0 are the intensities of a labile proton signal with and without saturation of the ^1H_2O signal, respectively. $T_{1(int)}$ is the intrinsic spin–lattice relaxation time, with which F is evaluated. τ_i is the lifetime of the labile proton in the protein environment, and hence $\tau_i^{-1} = k_{ex}$. Consequently, independent measurements of $T_{1(int)}$ and F allow the determination of k_{ex}.

If $T_{1(int)}$ is independently known and remains constant over the pH range used, k_{ex} is obtained through Eq. (18.20′).

$$k_{ex} = \tau_i^{-1} = T_{1(int)}^{-1} \times (1 - F)F^{-1} \tag{18.20'}$$

With the occurrence of exchange, and when $T_{1(int)}$ cannot be determined directly, k_{ex} is obtained through Eq. (18.21).

$$k_{ex} = T'^{-1}_{1(int)} \times (1 - F) \tag{18.21}$$

where $T'^{-1}_{1(int)} = T_{1(int)}^{-1} + \tau_i^{-1}$. In such a case, $T_{1(int)}$ can be expressed as

$$T_{1(int)}^{-1} = F \times T'^{-1}_{1(int)} \tag{18.22}$$

$T_{1(\mathrm{int})}$ can be measured as follows. At pH values where τ_i of the labile proton is long compared with $T_{1(\mathrm{int})}$, i.e., $T_{1(\mathrm{int})} \ll \tau_i$, a selective saturation recovery experiment with a pulse sequence for solvent suppression is performed. At pH values where $\tau_i \approx T_{1(\mathrm{int})}$, $T'^{-1}_{1(\mathrm{int})}$ is obtained by selective inversion recovery with the saturation of the H_2O signal at all times except during acquisition.

In general, k_{ex} is expressed as [118]

$$k_{\mathrm{ex}} = k_A[\mathrm{H}^+]^A + k_B[\mathrm{OH}^-]^B + k_W[\mathrm{H_2O}] \tag{18.23}$$

where k_A, k_B, and k_W are the rate constants for H^+, OH^-, and H_2O catalysis, respectively. Exponents A and B are at unity with k_A and k_B close to those observed for a model compound and are less than unity for protons buried in the protein interior and/or involved in hydrogen bonds [118]. When k_A and k_B are comparable in magnitude to each other, the pH value at the minimum k_{ex} is close to $\sim$7. A change in either k_A or k_B alters the pH value at the minimum k_{ex} [118].

For example, the His93 $N_\delta H$ proton signal of deoxy Mb is observed at $\sim$75 ppm [96] (trace 2D). The His93 $N_\delta H$ proton of the protein is hydrogen-bonded to the carbonyl oxygen atom of Leu89, as illustrated in Fig. 18.1c, and exhibits $T_{1(\mathrm{int})} = \sim 15$ ms and $k_{\mathrm{ex}} = \sim 30\ \mathrm{s}^{-1}$ at pH = 10.6 and 40 °C. Interestingly, the k_{ex} value of the His93 $N_\delta H$ protons of the subunits of the deoxy form of tetrameric human adult hemoglobin, i.e., $k_{\mathrm{ex}} = \sim 10^{-4}$–$10^{-5}\ \mathrm{s}^{-1}$, is several orders of magnitude smaller than that of deoxy Mb [122].

A 400 MHz ^{1}H NMR spectrum of bovine metMbCN$^-$ at 25 °C is shown in Fig. 18.11. In the spectrum, His64 $N_\varepsilon H$ and His93 $N_\delta H$ proton signals were

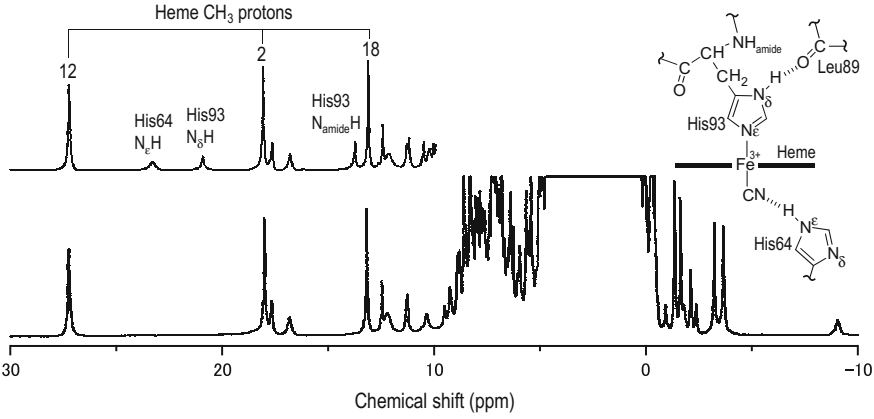

Fig. 18.11 400 MHz ^{1}H NMR spectrum of bovine metMb (CN^-) in 90% ^1H_2O/10% ^2H_2O, pH 7.0, at 25 °C. The downfield-shifted portion of the spectrum of the protein in ^2H_2O, pH 7.0, at 25 °C is shown in *the inset*. Assignments of 2-, 12-, and 18-CH_3 signals and His64 $N_\varepsilon H$, His93 $N_\delta H$, and His93 $N_{\mathrm{amide}}H$ ones are shown in the spectrum. The location of these NH protons in the protein is shown in *the inset*. The spectra were taken from [123]

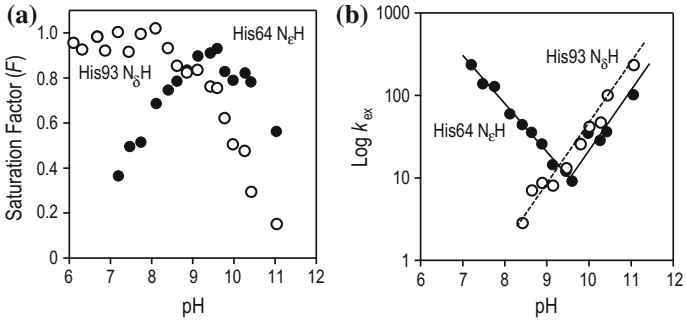

Fig. 18.12 pH-profiles of **a** saturation factor (F) and **b** logarithm of k_{ex} (s^{-1}) for the His64 $N_{\varepsilon}H$ (*filled circle*) and His93 $N_{\delta}H$ protons (*open circle*) in bovine metMbCN^{-} in 90% $^{1}H_2O$/10% $^{2}H_2O$ at 25 °C [123]. The exchange behavior of histidyl imidazole ring NH hydrogen atoms sharply reflects their local environment. The H^{+} and OH^{-} catalyses involve an attack at different sites of the neutral imidazole side chain, and both acid- and base-catalyzed exchanges were observed for the His64 $N_{\varepsilon}H$ proton. On the other hand, only base-catalyzed exchange was observed for the His93 $N_{\delta}H$ proton because of the coordination of His93 to heme Fe, which precludes acid-catalyzed exchange

observed at 23.31 and 20.96 ppm, respectively, and exhibited $T_{1(int)}$ values of 8.4 and 22 ms, respectively [123]. The F values of the His64 $N_{\varepsilon}H$ and His93 $N_{\delta}H$ protons of the protein at various pH values were measured (Fig. 18.12a), and then, the pH-profiles of the k_{ex} values of the protons were calculated from the F and $T_{1(int)}$ values [123] (Fig. 18.12b). The k_{ex} values of the His64 $N_{\varepsilon}H$ and His93 $N_{\delta}H$ protons exhibited distinctly different pH-profiles. The pH-profile of the k_{ex} value of the His64 $N_{\varepsilon}H$ proton reflected both acid- and base-catalyzed NH hydrogen exchange, with the minimum k_{ex} value at pH $\sim$9.5. On the other hand, only the base-catalyzed exchange was manifested in the pH-profile of the k_{ex} value of His93 $N_{\delta}H$ hydrogen atom. Thus, the k_{ex} values of the NH protons provide valuable information about the dynamic nature of the heme cavity of the protein.

18.5 Concluding Remarks

This chapter has described the fundamentals of ^{1}H NMR spectra of paramagnetic compounds. Using Mb as a reference compound, the spectral characteristics of paramagnetic compounds possessing a series of S values have been described in order to provide an overview of the effects of changes in the number of unpaired electrons on the spectral features. A few techniques applied to paramagnetic compounds, which provide widespread utility in life and material sciences, have also been described. As described in this chapter, the use of electron spin is opening up new horizons for NMR studies in life and material sciences.

Acknowledgements The authors are grateful to Professor Toshiyuki Tanaka (Graduate School of Life and Environmental Sciences, University of Tsukuba) for the use of a Bruker AVANCE III 800 spectrometer at TARA Center, University of Tsukuba.

References

1. Wüthrich, K.: Structural studies of hemes and hemoproteins by nuclear magnetic resonance spectroscopy. Struct. Bond. **8**, 53–121 (1970)
2. La, M.G.N., Horrocks, W.D.W., Holm, R.H. (eds.): NMR of Paramagnetic Molecules, Principles and Applications. Academic Press, New York (1973)
3. Morrow, J.S., Gurd, F.R.N.: Nuclear magnetic resonance studies of hemoglobin: functional state correlations and isotopic enrichment strategies. CRC Crit. Rev. Biochem. **3**, 221–287 (1975)
4. Wüthrich, K.: NMR in Biological Research: Peptides and Proteins, Chap. 6. North-Holland Publishing, Amsterdam (1976)
5. Morishima, I., Ogawa, S., Inubushi, T., Iizuka, T.: Nuclear magnetic resonance studies of high-spin ferric hemoproteins. Adv. Biophys. **11**, 217–245 (1978)
6. La Mar, G.N.: Model compound as aids in interpreting NMR spectra of hemoproteins. In: Shulman, R.G. (ed.) Biological Application of Magnetic Resonance, pp. 305–343. Academic Press, New York (1979)
7. Inagaki, F., Miyazawa, T.: NMR analyses of molecular conformations and conformational equilibria with the lanthanide probe method. Prog. NMR Spectrosc. **14**, 67–111 (1981)
8. Keller, R.M., Wüthrich, K.: Multiple irradiation ^{1}H NMR experiments with hemopoteins. Biol. Magn. Reson. **3**, 1–51 (1981)
9. Jardetzky, O., Roberts, G.C.K.: NMR in Molecular Biology, Chap. III. Academic Press, New York, pp. 69–114 (1981)
10. Bertini, I., Luchinat, C.: NMR of Paramagnetic Molecules in Biological Systems. Benjamin/Cummings Publishing, Menlo Park (1986)
11. Satterlee, J.D.: MNR spectroscopy of paramagnetic haem proteins. Annu. Rep. NMR Spectrosc. **17**, 79–178 (1986)
12. Satterlee, J.D.: Proton NMR studies of biological problems involving paramagnetic heme proteins. Met. Ions Biol. Syst. **21**, 121–185 (1986)
13. Bertini, I., Turano, P., Vila, A.J.: Nuclear magnetic resonance of paramagnetic metalloproteins. Chem. Rev. **93**, 2833–2932 (1993)
14. Yamamoto, Y.: NMR study of active sites in paramagnetic haemoproteins. Annu. Rep. NMR Spectrosc. **36**, 1–77 (1998)
15. La Mar, G.N., Satterlee, J.D., de Ropp, J.S.: Nuclear magnetic resonance of hemoproteins. In: Kadish, K.M., Smith, K.M., Guilard, R. (eds.) The Porphyrin Handbook, pp. 185–298. Academic Press, San Diego (2000)
16. Bertini, I., Luchinat, C., Parigi, G.: Solution NMR of Paramagnetic Molecules. Elsevier, Amsterdam (2001)
17. de Ropp, J.S., Yu, L.P., La Mar, G.N.: 2D NMR of paramagnetic metalloenzymes: cyanide-inhibited horseradish peroxidase. J. Biomol. NMR **1**, 175–190 (1991)
18. Banci, L., Piccioli, M., Scozzafava, A.: Advances in the NMR investigation of paramagnetic molecules in solution. Coord. Chem. Rev. **120**, 1–28 (1992)
19. Ubbink, M., Worrall, J.A.R., Canters, G.W., Groenen, E.J.J., Huber, M.: Paramagnetic resonance of biological metal centers. Annu. Rev. Biophys. Biomol. Struct. **31**, 393–422 (2002)
20. Amesano, F., Banci, L., Piccioli, M.: NMR structures of paramagnetic metalloproteins. Q. Rev. Biophys. **38**, 167–219 (2005)

21. Bertini, I., Luchinat, C., Parigi, G., Pierattelli, R.: NMR spectroscopy of paramagnetic metalloproteins. ChemBioChem **6**, 1536–1549 (2005)
22. Tang, C., Iwahara, J., Clore, G.M.: Visualization of transient encounter complexes in protein-protein association. Nature **444**, 383–386 (2006)
23. Clore, G.M., Tang, C., Iwahara, J.: Elucidating transient macromolecular interactions using paramagnetic relaxation enhancement. Curr. Opin. Struct. Biol. **17**, 603–616 (2007)
24. Tang, C., Schwieters, C.D., Clore, G.M.: Open-to-closed transition in apo maltose-binding protein observed by paramagnetic NMR. Nature **449**, 1078–1082 (2007)
25. John, M., Schmitz, C., Park, A.Y., Dixon, N.E., Huber, T., Otting, G.: Sequence-specific and stereospecific assignment of methyl groups using paramagnetic lanthanides. J. Am. Chem. Soc. **129**, 13749–13757 (2007)
26. Pintacuda, G., John, M., Su, X.C., Otting, G.: NMR structure determination of protein–ligand complexes by lanthanide labeling. Acc. Chem. Res. **40**, 206–212 (2007)
27. Bertini, I., Luchinat, C., Parigi, G., Pierattelli, R.: Perspectives in paramagnetic NMR of metalloproteins. Dalton Trans. **29**, 3782–3790 (2008)
28. Clore, G.M., Iwahara, J.: Theory, practice, and applications of paramagnetic relaxation enhancement for the characterization of transient low-population states of biological macromolecules and their complexes. Chem. Rev. **109**, 4108–4139 (2009)
29. Otting, G.: Protein NMR using paramagnetic ions. Annu. Rev. Biophys. **39**, 387–405 (2010)
30. Bertini, I., Emsley, L., Lelli, M., Luchinat, C., Mao, J., Pintacuda, G.: Ultrafast MAS solid-state NMR permits extensive ^{13}C and ^{1}H detection in paramagnetic metalloproteins. J. Am. Chem. Soc. **132**, 5558–5559 (2010)
31. Iwahara, J., Clore, G.M.: Structure-independent analysis of the breadth of the positional distribution of disordered groups in macromolecules from order parameters for long, variable-length vectors using NMR paramagnetic relaxation enhancement. J. Am. Chem. Soc. **132**, 13346–13356 (2010)
32. Bertini, I., Giachetti, A., Luchinat, C., Parigi, G., Petoukhov, M.V., Pierattelli, R., Ravera, E., Svergun, D.I.: Conformational space of flexible biological macromolecules from average data. J. Am. Chem. Soc. **132**, 13553–13558 (2010)
33. Ravera, E., Salmon, L., Fragai, M., Parigi, G., Al-Hashimi, H., Luchinat, C.: Insights into domain-domain motions in proteins and RNA from solution NMR. Acc. Chem. Res. **47**, 3118–3126 (2014)
34. Yamaguchi, T., Sakae, Y., Zhang, Y., Yamamoto, S., Okamoto, Y., Kato, K.: Exploration of conformational spaces of high-mannose-type oligosaccharides by an NMR-validated simulation. Angew. Chem. Int. Ed. Engl. **53**, 10941–10944 (2014)
35. Brath, U., Swamy, S.I., Veiga, A.X., Tung, C.-C., Van Petegem, F., Erdélyi, M.: Paramagnetic ligand tagging to identify protein binding sites. J. Am. Chem. Soc. **137**, 11391–11398 (2015)
36. Schlagnitweit, J., Tang, M., Baias, M., Richardson, S., Schantz, S., Emsley, L.: Nanostructure of materials determined by relayed paramagnetic relaxation enhancement. J. Am. Chem. Soc. **137**, 12482–12485 (2015)
37. Matei, E., Gronenborn, A.M.: ^{19}F paramagnetic relaxation enhancement: a valuable tool for distance measurements in proteins. Angew. Chem. Int. Ed. Engl. **55**, 150–154 (2016)
38. Ravera, E., Luchinat, C., Parigi, G.: Basic facts and perspectives of Overhauser DNP NMR. J. Magn. Reson. **264**, 78–87 (2016)
39. Kato, K., Yamaguchi, T.: Paramagnetic NMR probes for characterization of the dynamic conformations and interactions of oligosaccharides. Glycoconj. J. **32**, 505–513 (2015)
40. Feintuch, A., Otting, G., Goldfarb, D.: Gd^{3+} spin labeling for measuring distances in biomacromolecules: why and how? Methods Enzymol. **563**, 415–457 (2015)
41. Bertmer, M.: Paramagnetic solid-state NMR of materials. Solid State Nucl. Magn. Reson. **81**, 1–7 (2017)
42. Chen, J.L., Wang, X., Yang, F., Cao, C., Otting, G., Su, X.C.: 3D structure determination of an unstable transient enzyme intermediate by paramagnetic NMR spectroscopy. Angew. Chem. Int. Ed. Engl. **55**, 13744–13748 (2016)

43. Pilla, K.B., Otting, G., Huber, T.: Pseudocontact shift-driven iterative resampling for 3D structure determinations of large proteins. J. Mol. Biol. **428**, 522–532 (2016)
44. Orton, H.W., Kuprov, I., Loh, C.-T., Otting, G.: Using paramagnetism to slow down nuclear relaxation in protein NMR. J. Phys. Chem. Lett. **7**, 4815–4818 (2016)
45. Pilla, K.B., Otting, G., Huber, T.: 3D computational modeling of proteins using sparse paramagnetic NMR data. Methods Mol. Biol. **1526**, 3–21 (2017)
46. Can, T.V., Ni, Q.Z., Griffin, R.G.: Mechanisms of dynamic nuclear polarization in insulating solids. J. Magn. Reson. **253**, 23–35 (2015)
47. Su, Y., Andreas, L., Griffin, R.G.: Magic angle spinning NMR of proteins: high-frequency dynamic nuclear polarization and ^{1}H detection. Annu. Rev. Biochem. **84**, 465–497 (2015)
48. Matsuki, Y., Idehara, T., Fukazawa, J., Fujiwara, T.: Advanced instrumentation for DNP-enhanced MAS NMR for higher magnetic fields and lower temperatures. J. Magn. Reson. **264**, 107–115 (2016)
49. Comment, A.: Dissolution DNP for in vivo preclinical studies. J. Magn. Reson. **264**, 39–48 (2016)
50. McConnell, H.M., Holm, C.H.: Proton resonance shifts in nickelocene. J. Chem. Phys. **27**, 314–315 (1957)
51. McConnell, H.M., Holm, C.H.: Proton resonance shifts in paramagnetic metal aromatic complexes. J. Chem. Phys. **28**, 749–750 (1958)
52. Bloembergen, N.: Proton relaxation times in paramagnetic solutions. J. Chem. Phys. **27**, 572–573 (1957)
53. McConnell, H.M., Chesnut, D.B.: Theory of isotropic hyperfine interactions in π-electron radicals. J. Chem. Phys. **28**, 107–117 (1958)
54. McConnell, H.M., Robertson, R.E.: Isotropic nuclear resonance shifts. J. Chem. Phys. **29**, 1361–1365 (1958)
55. Karplus, M.: Contact electron-spin coupling of nuclear magnetic moments. J. Chem. Phys. **30**, 11–15 (1959)
56. Abragam, A.: The Principles of Nuclear Magnetism. Oxford University Press, Oxford (1961)
57. Karplus, M., Fraenkel, G.K.: Theoretical interpretation of carbon-13 hyperfine interactions in electron spin resonance spectra. J. Chem. Phys. **35**, 1312–1323 (1961)
58. Fitzgerald, R.J., Drago, R.S.: Contact-shift studies and delocalization mechanisms of nickel (II)-benzylamine complexes. J. Am. Chem. Soc. **89**, 2879–2883 (1967)
59. Fitzgerald, R.J., Drago, R.S.: Contact-shift studies, delocalization mechanisms, and extended Hückel calculations of nickel(II)-alkylamine complexes. J. Am. Chem. Soc. **90**, 2523–2527 (1968)
60. Kurland, R., McGarvey, B.R.: Isotropic NMR shifts in transition metal complexes: the calculation of the Fermi contact and pseudocontact terms. J. Magn. Reson. **2**, 286–301 (1970)
61. Abragam, A., Bleaney, B.: Electron Paramagnetic Resonance of Transition Metal Ions. Oxford University Press, Oxford (1970)
62. Schwarzhans, K.E.: NMR spectroscopy of paramagnetic complexes. Angew. Chem. Int. Ed. Engl. **9**, 946–953 (1970)
63. Crans, D.C., Yang, L., Gaidamauskas, E., Khan, R., Jin, W., Simonis, U.: Applications of paramagnetic NMR spectroscopy for monitoring transition metal complex stoichiometry and speciation. In: Telser, J. (ed.) Paramagnetic Resonance of Metallobiomolecules, ACS Book Series 858, pp. 304–326. American Chemical Society, Washington (2003)
64. Bertini, I., Luchinat, C., Parigi, G., Ravera, E.: NMR of Paramagnetic Molecules, Applications to Metallobiomolecules and Models, 2nd edn. Elsevier Science, Amsterdam (2016)
65. Walker, F.A.: Magnetic spectroscopic (EPR, ESEEM, Mössbauer, MCD and NMR) studies of low-spin ferriheme centers and their corresponding heme proteins. Coord. Chem. Rev. **185–186**, 471–534 (1999)

66. Kendrew, J.C., Bodo, G., Dintzis, H.M., Parrish, R.G., Wyckoff, H., Phillips, D.C.: A three-dimensional model of the myoglobin molecule obtained by x-ray analysis. Nature **181**, 662–666 (1958)
67. Kowalsky, A.: Nuclear magnetic resonance studies of cytochrome *c*. Possible electron delocalization. J. Biol. Chem. **237**, 1807–1819 (1962)
68. Shulman, R.G., Wüthrich, K., Yamane, T., Antonini, E., Brunori, M.: Nuclear magnetic resonances of reconstituted myoglobins. Proc. Natl. Acad. Sci. U S A **63**, 623–628 (1969)
69. Wüthrich, K., Shulman, R.G., Peisach, J.: High-resolution proton magnetic resonance spectra of sperm whale cyanometmyoglobin. Proc. Natl. Acad. Sci. U S A **60**, 373–380 (1968)
70. Ogawa, S., Shulman, R.G., Yamane, T.: High resolution nuclear magnetic resonance spectra of hemoglobin. I. The cyanide complexes of α and β chains. J. Mol. Biol. **70**, 291–300 (1972)
71. La Mar, G.N., Budd, D.L., Viscio, D.B., Smith, K.M., Langry, K.C.: Proton nuclear magnetic resonance characterization of heme disorder in hemoproteins. Proc. Natl. Acad. Sci. U S A **75**, 5755–5759 (1978)
72. Morishima, I., Iizuka, T.: Nuclear magnetic resonance studies of hemoproteins. Unusual temperature dependence of hyperfine shifts and spin equilibrium in ferric myoglobin and hemoglobin derivatives. J. Am. Chem. Soc. **96**, 5279–5283 (1974)
73. Tolman, J.R., Flanagan, J.M., Kennedy, M.A., Prestegard, J.H.: Nuclear magnetic dipole interactions in field-oriented proteins: Information for structure determination in solution. Proc. Natl. Acad. Sci. U S A **92**, 9279–9283 (1995)
74. Tjandra, N., Omichinski, J.G., Gronenborn, A.M., Clore, G.M., Bax, A.: Use of dipolar ^{1}H-^{15}N and ^{1}H-^{13}C couplings in the structure determination of magnetically oriented macromolecules in solution. Nat. Struct. Biol. **4**, 732–738 (1997)
75. Antonini, E., Brunori, M.: Hemoglobin and Myoglobin in Their Reactions with Ligands. North Holland Publishing, Amsterdam (1971)
76. Takano, T.: Structure of myoglobin refined at 2.0 Å resolution. I. Crystallographic refinement of metmyoglobin from sperm whale. J. Mol. Biol. **110**, 537–568 (1977)
77. Takano, T.: Structure of myoglobin refined at 2.0 Å resolution. II. Structure of deoxy myoglobin from sperm whale. J. Mol. Biol. **110**, 569–584 (1977)
78. Vojtechovský, J., Chu, K., Berendzen, J., Sweet, R.M., Schlichting, I.: Crystal structures of myoglobin-ligand complexes at near-atomic resolution. Biophys. J. **77**, 2153–2174 (1999)
79. Hong, S., Sutherlin, K.D., Park, J., Kwon, E., Siegler, M.A., Solomon, E.I., Nam, W.: Crystallographic and spectroscopic characterization and reactivities of a mononuclear non-haem iron(III)-superoxo complex. Nat. Commun. **5**, 5440–5446 (2014)
80. Neya, S., Funasaki, N.: Proton nuclear magnetic resonance investigation of the spin-state equilibrium of the α and β subunits in intact azidomethemoglobin. Biochemistry **25**, 1221–1226 (1986)
81. Shibata, T., Kanai, Y., Nishimura, R., Xu, L., Moritaka, Y., Suzuki, A., Neya, S., Nakamura, M., Yamamoto, Y.: Characterization of ground state electron configurations of high-spin quintet ferrous heme iron in deoxy myoglobin reconstituted with trifluoromethyl group-substituted heme cofactors. Inorg. Chem. **55**, 12128–12136 (2016)
82. Solomon, I.: Relaxation processes in a system of two spins. Phys. Rev. **99**, 559–565 (1955)
83. Gueron, M.: Nuclear relaxation in macromolecules by paramagnetic ions: a novel mechanism. J. Magn. Reson. **19**, 58–66 (1975)
84. Vega, A.J., Fiat, D.: Nuclear relaxation processes of paramagnetic complexes the slow-motion case. Mol. Phys. **31**, 347–355 (1976)
85. Unger, S.W., Jue, T., La Mar, G.N.: Proton NMR dipolar relaxation by delocalized spin density in low-spin ferric porphyrin complexes. J. Magn. Reson. **61**, 448–456 (1985)
86. Yamamoto, Y.: Analysis of ^{13}C relaxation of heme peripheral methyl group in ferric low-spin myoglobin. J. Magn. Reson. B **103**, 72–76 (1994)

87. Mabbutt, B.C., Wright, P.E.: Assignment of heme and distal amino acid resonances in the ^{1}H-NMR spectra of the carbon monoxide and oxygen complexes of sperm whale myoglobin. Biochim. Biophys. Acta **832**, 175–185 (1985)
88. Emerson, S.D., La Mar, G.N.: Solution structural characterization of cyanometmyoglobin: resonance assignment of heme cavity residues by two-dimensional NMR. Biochemistry **29**, 1545–1556 (1990)
89. La Mar, G.N., Budd, D.L., Smith, K.M., Langry, K.C.: Nuclear magnetic resonance of high-spin ferric hemoproteins. Assignment of proton resonances in met-aquo myoglobins using deuterium-labeled hemes. J. Am. Chem. Soc. **102**, 1822–1827 (1980)
90. Unger, S.W., Lecomte, J.T.J., La Mar, G.N.: The utility of the nuclear Overhauser effect for peak assignment and structure elucidation in paramagnetic proteins. J. Magn. Reson. **64**, 521–526 (1985)
91. Yamamoto, Y., Chujo, R., Suzuki, T.: NMR study of *Galeorhinus japonicus* myoglobin. ^{1}H-NMR evidence for a structural alteration on the active site of *G. japonicus* myoglobin upon azide ion binding. Eur. J. Biochem. **198**, 285–291 (1991)
92. Beetlestone, J., George, P.: A magnetochemical study of equilibria between high and low spin states of metmyoglobin complexes. Biochemistry **3**, 707–714 (1964)
93. Iizuka, T., Kotani, M.: Analysis of a thermal equilibrium phenomenon between high-spin and low-spin states of ferrimyoglobin azide. Biochim. Biophys. Acta **154**, 417–419 (1968)
94. Neya, S., Morishima, I.: Interaction of methemoglobin with inositol hexaphosphate. Presence of the T state in human adult methemoglobin in the low spin state. J. Biol. Chem. **256**, 793–798 (1981)
95. Yamamoto, Y., Iwafune, K., Chujo, R., Inoue, Y., Imai, K., Suzuki, T.: ^{1}H-NMR comparative study of the active site in shark (*Galeorhinus japonicus*), horse, and sperm whale deoxy myoglobins. J. Biochem. **112**, 414–420 (1992)
96. La Mar, G.N., Davis, L., Johnson, R.D., Smith, W.S., Hauksson, J.B., Budd, D.L., Dalichow, F., Langry, K.C., Morris, I.K., Smith, K.M.: Nuclear magnetic resonance investigation of the electronic structure of deoxymyoglobin. J. Am. Chem. Soc. **115**, 3869–3876 (1993)
97. Bertin, I., Luchinat, C., Turano, P., Battaini, G., Casella, L.: The magnetic properties of myoglobin as studied by NMR spectroscopy. Chem. Eur. J. **9**, 2316–2322 (2003)
98. La Mar, G.N., Budd, D.L., Goff, H.: Assignment of proximal histidine proton NMR peaks in myoglobin and hemoglobin. Biochem. Biophys. Res. Commun. **77**, 104–110 (1977)
99. Thériault, Y., Pochapsky, T.C., Dalvit, C., Chiu, M.L., Sligar, S.G., Wright, P.E.: ^{1}H and ^{15}N resonance assignments and secondary structure of the carbon monoxide complex of sperm whale myoglobin. J. Biomol. NMR **4**, 491–504 (1994)
100. Yamamoto, Y.: ^{1}H NMR probes for inter-segmental hydrogen bonds in myoglobins. J. Biochem. **120**, 126–132 (1996)
101. Bougault, C.M., Dou, Y., Ikeda-Saito, M., Langry, K.C., Smith, K.M., La Mar, G.N.: Solution ^{1}H NMR study of the electronic structure and magnetic properties of high-spin ferrous or deoxy myoglobins. J. Am. Chem. Soc. **120**, 2113–2123 (1998)
102. Nishimura, R., Shibata, T., Tai, H., Ishigami, I., Yanagisawa, S., Ogura, T., Neya, S., Suzuki, A., Yamamoto, Y.: Effect of the electron density of the heme Fe atom on the Fe–histidine coordination bond in deoxy myoglobin. Bull. Chem. Soc. Jpn **87**, 905–911 (2014)
103. La Mar, G.N., de Ropp, J.S.: Proton NMR characterization of the state of protonation of the axial imidazole in reduced horseradish peroxidase. J. Am. Chem. Soc. **104**, 5203–5206 (1982)
104. Matsukawa, S., Mawatari, K., Yoneyama, Y., Kitagawa, T.: Correlation between the iron-histidine stretching frequencies and oxygen affinity of hemoglobins. A continuous strain model. J. Am. Chem. Soc. **107**, 1108–1113 (1985)
105. Johnson, M.E., Fung, L.W.-M., Ho, C.: Magnetic field and temperature induced line broadening in the hyperfine-shifted proton resonances of myoglobin and hemoglobin. J. Am. Chem. Soc. **99**, 1245–1250 (1977)

106. Emerson, S.D., La Mar, G.N.: NMR determination of the orientation of the magnetic susceptibility tensor in cyanometmyoglobin: a new probe of steric tilt of bound ligand. Biochemistry **29**, 1556–1566 (1990)
107. Yamamoto, Y., Nanai, N., Chujo, R., Suzuki, T.: Heme methyl hyperfine shift pattern as a probe for determining the orientation of the functionally relevant proximal histidyl imidazole with respect to the heme in hemoproteins. FEBS Lett. **264**, 113–116 (1990)
108. La Mar, G.N., Walker, F.A.: Proton nuclear magnetic resonance line widths and spin relaxation in paramagnetic metalloporphyrins of chromium(III), manganese(III), and iron (III). J. Am. Chem. Soc. **95**, 6950–6956 (1973)
109. La Mar, G.N., de Ropp, J.S., Smith, K.M., Langry, K.C.: Proton nuclear magnetic resonance investigation of the electronic structure of compound I of horseradish peroxidase. J. Biol. Chem. **256**, 237–243 (1981)
110. Yamamoto, Y., Osawa, A., Inoue, Y., Chujo, R.: A ^{1}H-NMR study of electronic structure of the active site of *Galeorhinus japonicus*. Eur. J. Biochem. **192**, 225–229 (1990)
111. Kao, Y.-H., Lecomte, J.T.J.: Determination of the zero-field splitting constant for proton NMR chemical shift analysis in metaquomyoglobin. The dipolar shift as a structural probe. J. Am. Chem. Soc. **115**, 9754–9762 (1993)
112. Trewhella, J., Wright, P.E., Appleby, C.A.: Molecular basis for proton-dependent anion binding by soybean leghaemoglobin *a*. Nature **280**, 87–88 (1979)
113. Johnson, R.D., Ramaprasad, S., La Mar, G.N.: A method of assigning functionally relevant amino acid residue resonances in paramagnetic hemoproteins using proton NOE measurements. J. Am. Chem. Soc. **105**, 7205–7206 (1983)
114. Plateau, P., Guéron, M.: Exchangeable proton NMR without base-line distortion, using new strong-pulse sequences. J. Am. Chem. Soc. **104**, 7310–7311 (1982)
115. Case, D.A., Karplus, M.: Dynamics of ligand binding to heme proteins. J. Mol. Biol. **132**, 343–368 (1979)
116. Karplus, M., McCammon, J.A.: The internal dynamics of globular proteins. CRC Crit. Rev. Biochem. **9**, 293–349 (1981)
117. McCammon, J.A., Karplus, M.: The dynamic picture of protein structure. Acc. Chem. Res. **16**, 187–193 (1983)
118. Woodward, C.K., Hilton, B.D.: Hydrogen exchange kinetics and internal motions in proteins and nucleic acids. Annu. Rev. Biophys. Bioeng. **8**, 99–127 (1979)
119. Krishna, M.M.G., Hoang, L., Lin, Y., Englander, S.W.: Hydrogen exchange methods to study protein folding. Methods **34**, 51–64 (2004)
120. Anthis, N.J., Clore, G.M.: Visualizing transient dark states by NMR spectroscopy. Q. Rev. Biophys. **48**, 35–116 (2015)
121. Lecomte, J.T.J., La Mar, G.N.: Proton NMR study of labile proton exchange in the heme cavity as a probe for the potential ligand entry channel in myoglobin. Biochemistry **24**, 7388–7395 (1985)
122. Han, K.-H., La Mar, G.N.: Nuclear magnetic resonance study of the isotope exchange of the proximal histidyl ring labile protons in hemoglobin A. The exchange rates and mechanisms of individual subunits in deoxy and oxy-hemoglobin. J. Mol. Biol. **189**, 541–552 (1986)
123. Yamamoto, Y., Kurihara, N., Egawa, T., Shimada, H., Ishimura, Y.: Hydrogen bonding interaction of the amide group of Asn and Gln at distal E7 of bovine myoglobin with bound-ligand and its functional consequences. Biochim. Biophys. Acta **1433**, 27–44 (1999)